The best composition of an Y-doped BaZrO electrolyte: Selection criteria from transport properties, microstructure, and phase behavior

AUTHOR(S):

Han, Donglin; Uda, Tetsuya

CITATION:

Han, Donglin ...[et al]. The best composition of an Y-doped BaZrO electrolyte: Selection criteria from transport properties, microstructure, and phase behavior. Journal of Materials Chemistry A 2018, 6(38): 18571-18582

ISSUE DATE:

2018-10-14

URL:

http://hdl.handle.net/2433/236378

To: Journal of Materials Chemistry A

Best Composition of Y-doped $BaZrO_3$ Electrolyte: Selection Criteria from Transport Properties, Microstructure, and Phase Behavior

Donglin Han *, Tetsuya Uda *

Department of Materials Science and Engineering, Kyoto University,

Yoshida Honmachi, Sakyo-ku, Kyoto 606-8501, Japan

* Corresponding authors: Donglin Han (han.donglin.8n@kyoto-u.ac.jp)

and Tetsuya Uda (uda_lab@aqua.mtl.kyoto-u.ac.jp)

TEL: +81-75-753-5445, FAX: +81-75-753-5284

Abstract

Y-doped $BaZrO_3$ shows high protonic conductivity in intermediate temperature, and has promising perspective to be applied as an electrolyte in electrochemical devices, including fuel cells and electrolysis cells. In this work, with the aim to determine the optimal composition of BZY for such electrochemical application, a thorough investigation on $BaZrO_3$ doped with 10 – 25 mol% Y with an interval of 1 mol% was performed, and the microstructure, phase behavior and transport properties were studied. The results revealed that after sintering at 1600 ^oC for 24 h, a bimodal microstructure was confirmed for $BaZr_{1-x}Y_xO_{3-\delta}$ (x = 0.10 – 0.15), whereas $BaZr_{1-x}Y_xO_{3-\delta}$ (x = 0.16 – 0.25) shows quite uniform grain size. Further investigation on BZY10, BZY15 and BZY20 by sintering at different time shows that uniform grain size around 2 and 6 μm were obtained for BZY15 and BZY20, respectively, but BZY10 still has a bimodal microstructure, even after sintering at 1600 ^oC for 200 h. Then through a systematic evaluation on the transport properties, we found that when the Y content is above 0.15, total conductivity over 0.01 Scm^{-1} is achieved even at 500 ^oC. And the transport number of ionic conduction in wet oxygen increases with the Y content increasing from 0.10 to 0.20, but does not further increase when the Y content is higher than 0.20. Notably, both Ba-deficiency and Ba-excess decrease the transport numbers of ionic conduction in wet oxygen. In conclusion, Y content around 0.20 with strictly controlled Ba stoichiometry seems to be the optimal composition.

1. Introduction

Fuel cells can convert the chemical energy in fossils, such as hydrogen, into electricity directly and efficiently. If they are operated reversely, namely, as electrolysis cells, hydrogen can be produced by electrolyzing water. Fuel cells and electrolysis cells are therefore expected to play important roles in the blueprint to establish a sustainable and green society by utilizing hydrogen as the medium for energy storage, transport and production. To some extent, the most important component in these electrochemical devices is the electrolyte, whose properties almost determine the operation conditions and strategy to implement or develop other components. In the case of using oxide ion conductive oxides as the electrolyte, *e.g.*, Y-stabilized ZrO_2 (YSZ), operation temperature above 800 ^oC is needed to generate sufficient oxide ion conductivity. Such high operation temperature results in tough challenges on material compatibility and uncertainty on long-term stability for cell operation.

Proton conductive oxides, firstly discovered by Iwahara, *et al.*[1, 2], provide a solution to lower the operation temperature to intermediate temperature range (400 – 700 ^oC), since the conduction of protons shows relatively low activation energy [3-6]. And currently, Y-doped $BaZrO_3$ (BZY) receives the most interest, due to its high proton conductivity (> 0.01 Scm^{-1} at 450 ^oC for $BaZr_{0.8}Y_{0.2}O_{3-\delta}$ [7, 8]) and significant chemical stability against carbon dioxide and water vapor [9, 10]. Potential to implement the BZY electrolyte into fuel cells [11-14] and electrolysis cells [15, 16] has been verified on bottom cells in a lab scale. However, reviewing the literature, these BZY electrolyte is almost limited to three compositions; $BaZr_{0.9}Y_{0.1}O_{3-\delta}$ (BZY10) [15, 17], $BaZr_{0.85}Y_{0.15}O_{3-\delta}$ (BZY15) [14, 18]

and $BaZr_{0.8}Y_{0.2}O_{3-\delta}$ (BZY20) [11-13, 16, 19-22]. And until now, which composition is the best one still remains as an open question. Fabbri, *et al*., investigated the samples doped with 20, 30, 40 and 50 mol% Y, and found that increasing the Y content from 20 mol% to 30 – 50 mol% did not help in increasing the proton conductivity [23]. A recent work in our group [8] screening the electroconductive properties of $BaZrO_3$ doped with 10, 15, 20 and 25 mol% Y, and found that 20 mol% Y imparted $BaZrO_3$ with relatively higher conductivity. If only focusing on the electrical conductivity, the Y doping level of 20 mol% appears to be good, but notably, the interval of Y content (5 [8] and 10 mol% [23]) in these previous research is still too large, and information on other compositions, especially those adjacent to the 20 mol% Y doped one, is lack, but no doubt of great importance.

Application as the electrolyte requires not only high electrical conductivity, but also high transport number of ionic conduction (t_{ion}). Although Y-doped $BaZrO_3$ shows pure ionic conduction (mainly proton) in wet hydrogen, significant contribution of hole conduction rises by exposing to wet oxygen. [24, 25] However, the reported values of t_{ion} discrete obviously even for the samples with the same nominal composition. For example, t_{ion} for $BaZr_{0.9}Y_{0.1}O_{3-\delta}$ and $BaZr_{0.8}Y_{0.2}O_{3-\delta}$ at 600 °C varied in the ranges of 0.38 – 0.67 [24, 26, 27, 28] and 0.4 – 0.52 [24, 25], respectively. The reason for such large discrepancy needs to be clarified. Furthermore, whether the transport properties of BZY can be tuned, for example, by simply changing the Y content, is an interesting topic needs to be discussed.

In this work, a systematic screening on the composition of BZY doped with Y content varying from 10 to 25 mol% with the interval of 1 at% was performed. In addition to the careful evaluation of the electrical conductivity and transport numbers of ionic conduction, change in phase behavior and microstructure with the composition and condition for heat-treatment was also investigated. Based on all the information collected, it is allowed to give answer to the question, what is the best composition of BZY for application as an electrolyte in fuel cells and electrolysis cells.

2. Experimental

2.1 Material Preparation

The $BaZr_{1-x}Y_xO_{3-\delta}$, and $BaZr_{0.8}M_{0.2}O_{3-\delta}$ (M = In, Ho, Er, Tm, Yb) samples were prepared by a conventional solid state reaction method. Starting materials of $BaCO_3$, ZrO_2, Y_2O_3, In_2O_3, Ho_2O_3, Er_2O_3, Tm_2O_3, and Yb_2O_3 were mixed at the desired ratio, and ball-milled for 24 h. After being pelletized under 9.8 MPa, the samples were heat-treated at 1000 ^oC for 10 h. Then, the samples were pulverized and ball-milled for 10 h, and pelletized under 9.8 MPa again, with a subsequent heat-treatment at 1300 ^oC for 10 h for synthesizing. The samples were pulverized and ball-milled for 100 h again, and pressed at 392 MPa into pellets with thickness and diameter around 1 mm and 11 mm, respectively. Finally, the resulting pellets were buried in sacrificial powder which is mixture of the as-synthesized powder and 1 wt% $BaCO_3$, and subjected to sintering at 1500, 1550 or 1600 ^oC in artificial oxygen atmosphere. The heating rate was 4.17 $^oCmin^{-1}$ from room temperature to 1000 ^oC,

and 3.33 ^{o}Cmin^{-1} from 1000 to the target temperature for sintering. The samples of $BaZr_{1-x}Y_xO_{3-\delta}$ (x = 0.10, 0.15 and 0.20) were quenched at room temperature in ambient atmosphere after the sintering performed at 1600 ^{o}C to see the phase behavior at 1600 ^{o}C, whereas the other samples were furnace cooled to the room temperature.

2.2 Characterization

Chemical compositions were determined by inductively coupled plasma atomic emission spectroscopy (ICP-AES) with SPS4000 (Seiko Instruments Inc., Chiba, Japan). The samples were dissolved in 0.1 mol/L nitric acid solution kept at around 80 ^{o}C with several droplets of concentrated hydrochloric acid. Microstructures were observed by electron probe microanalyzer (EPMA) with JXA-8530F (JEOL, Tokyo, Japan). Powder X-ray diffraction (XRD) measurements were performed using Cu $K\alpha$ radiation with X'Pert PRO MPD or Cu $K\alpha_1$ monochromatic radiation with X'Pert PRO Alpha-1 (PANalytical, Almelo, Netherland). Rietveld refinement was carried out utilizing a commercial software X'Pert HighScore Plus to determine lattice constants. Relative density of the as-sintered pellet-like samples was estimated with Archimedes method.

Conductivity measurements of the pellet-like samples with sputtered platinum (Pt) electrodes were performed in wet atmospheres of hydrogen, oxygen or those diluted with argon. The partial pressure of water vapor in the wet atmosphere was 0.05 atm obtained by bubbling the gas through deionized water kept at 33 ^{o}C. All the samples were fixed in alumina rings with zirconia cement (S-301, Asahi

Chemical Co., Ltd., Osaka, Japan) to improve the mechanical strength. Pt plates wiped with silver mesh were used as current collector. Pt wire was used to lead the current to a frequency response analyzer (Solartron SI 1260, Solartron Analytical, Farnborough, UK). The impedance spectra were collected in the frequency range from 10 Hz to 7 MHz with applied voltage of 100 mV. For completing the Arrhenius plots, the impedance spectra were collected every 50 min by cooling from 700 to 100 ^{o}C at 0.2 ^{o}Cmin^{-1}. For evaluating the transport numbers of ionic conduction, another sample was used to collect the impedance spectra at only three specific temperatures of 500, 600 and 700 ^{o}C, with relaxation time around 10 h and 1 h for changing temperature and atmosphere, respectively. A commercial software ZView (Scribner Associates, Inc., USA) was used to analyze the impedance spectra. The semicircles belonging to bulk and grain boundary resistance were determined by their specific capacitance of 10^{-11} and 10^{-9} F, respectively, and also a continuous change of the profile of the spectra with the change in temperature (Fig. S1). The resistances of bulk and grain boundary are determined by reading the value at the valley between adjacent two semicircles. And the total resistance was determined by reading the value at the valley between the grain boundary and electrode.

3. Results

3.1 Microstructure Observation and Phase Identification

(1) $BaZr_{1-x}Y_xO_{3-\delta}$ (x = 0 – 0.25) sintered at 1600 ^{o}C for 24 h

The EPMA second electron (EPMA-SE) images of the microstructure of $BaZrO_3$ doped with various amount of Y after sintering at 1600 °C in oxygen for 24 h are shown in **Fig. 1**. For the samples with the Y content between 0.10 and 0.13, a clear bimodal microstructure, which is a mixture of large grains (typically larger than 1 μm) and fine grains (typically around the order of 100 nm), was observed. The samples with the Y content of 0.14 and 0.15 also show a bimodal microstructure, but the ratio of the large grains greatly increases. With the Y content increasing to 0.16 - 0.25, the grain size turned to be uniform, and appears to increase with the increasing Y content.

From powder XRD patterns (**Fig. S2**), only diffraction peaks belonging to perovskite-type phases were confirmed. A single cubic perovskite-type structure ($Pm\bar{3}m$) model [29, 30] was then used to calculate the lattice constant. It should be noted here that since for some compositions (*e.g.*, $BaZr_{0.9}Y_{0.1}O_{3-\delta}$), more than one perovskite-type phases possibly co-exist after sintering at 1600 °C for 24 h, which will be described in the following section, the lattice constants thereby estimated using a single perovskite-type structure model reflect an average influence from all the co-existed perovskite phases. As shown in **Fig. 2**, in which our previously reported data on the system doped with small amount of Y below 0.05 [8, 31, 32] were also plotted, one can see that the lattice constants increase almost linearly with the increasing Y content, obeying the Vegard's law, since the radius of six-coordinated trivalent Y cations (0.900 Å [33]) is larger than that of tetravalent Zr cations (0.72 Å [33]).

(2) $BaZr_{1-x}Y_xO_{3-\delta}$ (x = 0.10, 0.15, 0.20) sintered at 1600 °C for different time

With regard to the formation of the bimodal microstructure, possible reasons include insufficient time for sintering, or the nature of such composition (*e.g.*, out of the compositional area for a single perovskite-type phase). Here, we selected three representative compositions of $BaZr_{0.9}Y_{0.1}O_{3-\delta}$ (BZY10), $BaZr_{0.85}Y_{0.15}O_{3-\delta}$ (BZY15) and $BaZr_{0.8}Y_{0.2}O_{3-\delta}$ (BZY20) for further investigation. The samples were quenched in ambient atmosphere from 1400 ^{o}C or 1500 ^{o}C on heating up, or after holding at 1600 ^{o}C for 0 – 200 h.

The images of the microstructure of the samples at each step during the sintering process are given in the Electronic Supplementary Information (EIS), and those of holding at 1600 ^{o}C for 4, 24, 100 and 200 h are picked out for example to show in **Fig. 3**. It is clear that for the BZY10 samples, the bimodal microstructure is kept even after heating at 1600 ^{o}C for 200 h. But it is noted that some grains grew with keeping bimodal microstructure. Although the microstructure of BZY15 appears to be bimodal after heating at 1600 ^{o}C for 4 h (**Fig. 3(e)**), the amount of the fine grains reduced obviously with the increasing heating time. After heating at 1600 ^{o}C for longer than 40 h, quite uniform grain size was observed, in agreement with the previous report in our group [34]. Extending the heating time to 200 h results in the grain size increasing to around 2 μm (**Fig. 3(h)**). The case of the BZY20 samples is similar, but even after heating at 1600 ^{o}C for 4 h, quite uniform grain size around 1 μm (**Fig. 3(i)**) was obtained. The grains further grow with the increasing heating time, and have the size around 2, 4 and 6 μm after keeping at 1600 ^{o}C for 24, 100 and 200 h.

XRD analysis with the monochromatic Cu *K*α1 radiation provides information on phase behaviour, as

shown in **Fig. 4**. The change in the shape of the (112) diffraction peak of BZY20 agrees with our previous reports [35]; that is, the lattice constant of the low temperature phase at 1300 ^{o}C is smaller than that of the high temperature phase at 1600 ^{o}C, and by heating the as-synthesized (1300 ^{o}C) BZY20 samples to 1600 ^{o}C, the low temperature phase entirely transformed to the high temperature phase. The behaviour of change in the peak shape of BZY15 is analogue to that of the BZY20. But, after heating the BZY15 and BZY20 samples at 1600 ^{o}C for 100 or 200 h, a small bump appears at the high angle side of the main peak, possibly due to the partial loss of BaO after annealing at 1600 ^{o}C for too long time, even these samples were buried in sacrificial powder.

The change in the shape of the (112) diffraction peak is different for the BZY10 samples. One can see that the peak shape is still quite broad and obviously asymmetric after heating at 1600 ^{o}C for 24 h, 40 h and 70 h. Such asymmetric appearance was most likely kept even after heating for 200 h, indicating that these BZY10 samples are possibly composed of at least two perovskite-type phases with different lattice constants. But clearly, by extending the sintering time, the intensity of the peak at the low angle side increases, and the intensity of the peak at the high angle side decreases, indicating that the perovskite-type phases with the larger lattice constant turns to predominate by heating at 1600 ^{o}C for sufficiently long time. Here, we simply assume the co-existence of two cubic perovskite-type phases, and the lattice constants are estimated through Rietveld refinement to be in the ranges of 4.196 – 4.203 Å and 4.206 – 4.211 Å, respectively, for the two phases. And the values are very close to those of the α (4.196 – 4.199 Å) and β (4.205 Å) phases reported by Azad, *et al* [36]. The change in

lattice constants of the perovskite phases, and relative density of BZY10, BZY15 and BZY20 with the proceeding of the sintering process is shown in **Fig. 5** and **S5**, respectively.

(3) $BaZr_{1-x}Y_xO_{3-\delta}$ (x = 0.20 – 0.25) sintered at 1500, 1550 and 1600 ^oC for 24 h

Since as shown in **Fig. 1**, the grain size of $Ba_{1-x}Y_xZrO_{3-\delta}$ (x = 0.20 – 0.25) is around 2 μm after sintering at 1600 ^oC for 24 h, we want to see whether good sinterability can also be acquired at lower temperature of 1500 and 1550 ^oC. As shown in **Fig. 6**, after sintering at 1500 ^oC, the grain size is not uniform and there are a lot of pores in the sample. However, the grains grow to the size around 1 μm, after sintering at 1550 ^oC for 24 h. And the relative density of the samples sintered at 1500 ^oC is below 93.5%, but increases over 95.5% after sintering at 1550 ^oC (**Fig. S7**). These results indicate that $BaZr_{1-x}Y_xO_{3-\delta}$ (x = 0.20 – 0.25) also show good sinterability after sintering even at 1550 ^oC for 24 h.

3.2 Transport number in wet oxygen

(1) Nominally stoichiometric $BaZr_{1-x}Y_xO_{3-\delta}$ (x = 0 – 0.25)

In this work, the transport number of ionic conduction (t_{ion}) in wet oxygen (p_{H_2O} = 0.05 atm) was estimated by evaluating the dependence of electrical conductivity on partial pressure of oxygen (p_{O_2}) following Eq. (1), since electronic holes ($h^\bullet$) are generated in oxidizing atmosphere as given in Eq. (2) [24, 25] and the hole concertation is assumed to be negligibly smaller than ionic defects. Here, σ_{total},

σ_{ion} and σ_h are the total, ionic and hole conductivities in wet oxygen, respectively, and $O_O^{\times}$ and $V_O^{\bullet\bullet}$ are oxide ions and oxide ion vacancies expressed in Kröger-Vink notation, respectively. Using σ_{ion} and σ_h obtained by fitting the experimental data with Eq. (1), one can calculate t_{ion} in wet oxygen with Eq. (3). An example of the fitting of σ_{total} of $BaZr_{0.8}Y_{0.2}O_{3-\delta}$ against p_{O_2} is shown in **Fig. 7**. The impedance spectra shift towards low real resistance side (an example at 600 °C is shown in the inset of **Fig. 7**), therefore σ_{total} increases, with the increasing p_{O_2}, indicating enhancement in σ_h with increasing p_{O_2}. [24, 25]

$$\sigma_{total} = \sigma_{ion} + \sigma_h (p_{O_2})^{\frac{1}{4}} \quad (1)$$

$$2V_O^{\bullet\bullet} + O_2 = 2O_O^{\times} + 4h^{\bullet} \quad (2)$$

$$t_{ion} = \frac{\sigma_{ion}}{\sigma_{ion} + \sigma_h (p_{O_2})^{\frac{1}{4}}} \quad (3)$$

Fig. 8 shows t_{ion} for nominally stoichiometric samples of $BaZrO_3$ doped with various amount of Y. For the samples prepared by the first batch, in general, t_{ion} tends to increase with the Y content increasing from 0.10 to 0.20 or 0.21. However, further increasing the Y content to 0.25 does not improve t_{ion}. Especially, t_{ion} of $BaZr_{0.77}Y_{0.23}O_{3-\delta}$ (BZY23) drops abnormally compared with the value of the adjacent compositions. To verify the reproducibility, two new batches of samples with the Y content between 0.21 and 0.24 were prepared and measured. However, quite obvious discrepancy was confirmed, for example, the values of t_{ion} of BZY23 prepared in the 1st, 2nd and 3rd batches were about 0.72, 0.79 and 0.77 at 600 °C, respectively.

(2) Off-stoichiometry in Ba content

With the aim to clarify the reason for the discrepancy in t_{ion}, we firstly measured the average composition of all the samples by ICP-AES measurements, as shown in **Table 1**. One can see that the Y and Zr contents coincide well with the nominal values, but the Ba content deviates from the stoichiometric value of unity in most cases. For example, the Ba content determined for BZY23 of the 1st, 2nd and 3rd batches are 0.96, 1.03 and 1.03, respectively. Since the evaporation of BaO becomes severe at 1600 ^{o}C, [37] even all the samples were buried in the sacrificial powder during sintering, a precise control on the Ba content with good reproducibility among different batches might be still difficult.

Next, 20 mol% Y-doped $BaZrO_3$ with deliberately introduced Ba-deficiency ($Ba_{0.95}Zr_{0.80}Y_{0.20}O_{3-\delta}$ and $Ba_{0.98}Zr_{0.80}Y_{0.20}O_{3-\delta}$) was prepared as the 4th batch. The transport numbers of ionic conduction in wet O_2 are shown in **Fig. 9** with the comparison of nominally stoichiometric BZY20. It is clear that with the increasing Ba deficiency, t_{ion} decreases obviously. Then, t_{ion} of the samples with the Y content between 0.20 and 0.25 at 600 ^{o}C was picked out, and plotted against the actual Ba content determined by ICP-AES (**Table 1**), as shown in **Fig. 10**. Here, Ba-excessive BZY20 with the nominal composition of $Ba_{1.02}Zr_{0.80}Y_{0.20}O_{3-\delta}$ was also prepared and measured. Quite apparently, from **Fig. 10**, one can see that t_{ion} increases with the composition approaching the stoichiometric value (namely, Ba content of unity) from the Ba-deficient and Ba-excessive region. These results clearly indicate a negative impact on the transport number of ionic conduction in wet oxygen from deviation of Ba

content from unity, and therefore it is very important to keep the stoichiometric composition to suppress the enhancement of hole conduction. The microstructures and conductivity of the samples of BZY20 with different Ba content studied in this work are shown in Electronic Supplementary Information.

(3) $BaZr_{0.8}M_{0.2}O_{3-\delta}$ (M = Y, In, Ho, Er, Tm or Yb)

In our previous work, we measured the transport numbers of different charge carriers in $BaZrO_3$ doped with various type of dopants, including In, Ho, Er, Tm or Yb, by the electromotive force method. [24] However, compensation on electrode polarization is needed since significant hole conduction generated in wet oxygen atmosphere, and this introduced quite large error. Here, we re-measured the transport number of ionic conduction in wet O_2 through a more reliable method by evaluating the dependence of total conductivity with the partial pressure of oxygen. As shown in **Fig. 11**, $BaZr_{0.8}Y_{0.2}O_{3-\delta}$ shows higher t_{ion} than the samples containing any other dopant. There is possibility that such difference in t_{ion} might be partially due to the deviation of Ba content from unity, for example, as given in **Table 1**, the actual Ba content of the In, Tm and Yb-doped samples are 1.03, 1.02 and 1.04, respectively. However, for the Ho and Er-doped samples, their actual Ba content are 1.00 and 0.99, respectively, comparable with that of BZY20 (Ba content is 0.99). And clearly, t_{ion} of the Ho and Er-doped samples is lower than that of BZY20. Therefore, Y is apparently better than In, Ho, Er, Tm or Yb to achieve higher t_{ion} in $BaZrO_3$.

3.3 Conductivity in wet hydrogen

(1) $BaZr_{1-x}Y_xO_{3-\delta}$ (x = 0.10, 0.15 and 0.20) sintered at 1600 °C for various time

Fig. 12 shows the bulk conductivities measured in wet H_2 (p_{H_2O} = 0.05 atm) for the BZY10 and BZY15 samples sintered by heating at 1600 °C for different time. The bulk conductivity of BZY10 sintered at 1600 °C for 24 h in this work is close to our previous report on the sample prepared with the same condition [8]. However, when the time for sintering was extended to 40 h, a dramatic decrease in the bulk conductivity of BZY10 occurred, and the bulk conductivity kept stable with the sintering time further increased to 70 and 100 h. In contrary, the bulk conductivities for BZY15 are very close though sintering time at 1600 °C varies from 4 to 100 h. Such results indicate that the intra-grain properties are stabilized for BZY15 after sintering for relatively short time (4 h), but is still changing for BZY10 between sintering for 24 and 40 h. This change is very interesting but it is difficult to explain at present stage.

Since the grains of BZY15 and BZY20 grow obviously with the increasing time for sintering (**Fig. 3**), it is interesting to see how such the change in microstructure influences the electrical conductivities. We therefore measured the conductivities of the samples sintered for 4, 24 and 100 h. Although the bulk conductivities only change slightly with different sintering time, as expected, the grain boundary conductivities, and therefore the total conductivities, increase with extending the sintering time (**Figs. S9** and **S10**).

(2) Nominally stoichiometric $BaZr_{1-x}Y_xO_{3-\delta}$ (x = 0 – 0.25)

The total conductivities of $BaZrO_3$ doped with different amount of Y collected at 500, 600 and 700 ^oC in wet H_2 are shown in **Fig. 13**. One can see that for the samples containing Y content between 0.15 and 0.25, the total conductivities exceed 0.01 Scm^{-1} even at 500 ^oC. In this work, the total conductivity of $BaZr_{0.85}Y_{0.15}O_{3-\delta}$ (BZY15) is higher than that reported in our previous work due to the relatively smaller ratio of the fine grains. And the difference in conductivities is quite small among the samples with different composition, when the Y content was higher than around 0.18. The Arrhenius plots of the bulk, grain boundary and total conductivities of all these samples are given in the Electronic Supplementary Information with the activation energy and pre-exponential factors for information.

4. Discussion

4.1 Correlation between conductivity and fabrication route of BZY10

With the time for sintering at 1600 ^oC increasing from 24 h to 40 – 100 h, the amount of the perovskite phase with larger lattice constant (4.206 – 4.211 Å) increases, and the bulk conductivity decreases obviously. By comparing the bulk conductivities of BZY10 and BZY15 heat-treated at 1600 ^oC for the same time between 40 – 100 h, one can see that the bulk conductivity of BZY15 is about one order of magnitude higher than that of BZY10. Since the protons ($OH_O^{\cdot}$) are introduced through hydration reaction (Eq. (4)) with the participant of oxide ion vacancies, whose composition is determined by the

Y content (Eq. (5)), the concentration of charge carriers of protons in BZY15 is nearly 1.5 times higher than that of BZY10 [4]. So, there should be some other reason for such large difference in the bulk conductivity between BZY10 and BZY15. We considered the possibility that it might be easier for BZY10 to lose BaO during sintering at 1600 °C, since the relative density of BZY10 is obviously lower than that of BZY15 or BZY20 (**Fig. S6**). By ICP-AES measurements, we found that with the sintering time extended to higher than 40 h, there is some Ba-deficiency, typically about 0.2 – 0.3 at 40 h, as shown in **Table S2**. However, the Ba-deficiency in BZY10 does not differ from that in BZY15 and BZY20. And such small amount of Ba-deficiency only decreases the bulk conductivity slightly [24, 38].

$$H_2O + V_O^{\cdot\cdot} + O_O^{\times} = 2OH_O^{\cdot} \quad (4)$$

$$2Zr_{Zr}^{\times} + Y_2O_3 + O_O^{\times} = 2ZrO_2 + 2Y_{Zr}^{'} + V_O^{\cdot\cdot} \quad (5)$$

A similar phenomenon was also observed by Asad, *et al.* on the BZY10 system [36], but they suggested that it was the phase with large lattice constant (β phase) which showed higher proton conductivity. Such conclusion is contrary to our observation in this work, since we found that by sintering at 1600 °C for longer time, the peak intensity of the phase with large lattice constant increased, but the bulk conductivity decreased. A summarization of the reported bulk conductivity of BZY10 is given in **Fig. S16** and **Table S1**. Comparison with the data reported by Azad, *et al*. [36] is difficult, since the relative density of their samples scatters greatly (65 – 94%). But, one can see that the bulk conductivity of BZY10 sintered at 1600 °C for 24 h in this work is close to that reported by Bohn, *et*

al (sintered at 1715 ºC for 30 h) [39], whereas the value of BZY10 after sintered for longer time is close to that reported by Kjølseth, *et al* (sintered at 1650 ºC for 1 h) [40]. Since information is limited, it is not easy to explain the conductivity difference of BZY10 between this work and literatures. We consider that with sintering temperature and time the properties of powder of BZY10 before sintering, *e.g.*, particle size, phases, uniformity of distribution of elements, should be took into account.

Anyhow, from the results obtained in this work, the phase relationship for the composition of $BaZr_{0.90}Y_{0.10}O_{3-\delta}$ appears to be complicated, compared with other ones, such as $BaZr_{0.85}Y_{0.15}O_{3-\delta}$ and $BaZr_{0.80}Y_{0.20}O_{3-\delta}$. A careful handling on the preparation of BZY10 is essential due to its sensitivity of electrical conductivity on the fabrication route and history for heat-treatment.

4.2 Influence of deviation of Ba content from stoichiometry on transport properties

In our previous study, we reported the transport numbers of various charge carriers, including protons, oxide ions, and holes, in $BaZr_{0.8}Y_{0.2}O_{3-\delta}$ with different Ba content by electromotive force measurements [24]. However, since the hole conduction is enhanced in the wet oxygen atmosphere, compensation on electrode polarization was performed. [41, 42] But unfortunately, such compensation introduced quite large error, and the difference on the transport number of ionic conduction in wet oxygen turns to be negligibly small among the samples with different Ba content. [24] Such conclusion was proved to be incorrect in this work by using a much more reliable method.

Both Ba-deficiency and Ba-excess deteriorate the contribution of ionic conduction in BZY with Y content varying from 0.20 – 0.25. When Ba-deficiency was introduced, both the bulk and grain boundary conductivities decreased. The reduction of grain boundary conductivity was explained by smaller grain sizes, and that of the bulk conductivity was explained by the decrease of yttrium contents in barium zirconate phases and plausibly formation of stacking faults [24, 38, 43]. The hole conductivities in wet O_2 at 600 ^oC in this study were calculated to be 0.0069, 0.0041 and 0.0015 Scm^{-1} for BZY20 with nominal Ba content of 1, 0.98 and 0.95, respectively. Since the hole conductivity also decreased, we can therefore conclude that the ionic conductivity decreases more than that of holes. Excessive Ba content in the nominal composition also results in decrease in t_{ion}. However, since the formation of vacancies in Zr/Y site is energetically unfavorable, the excessive Ba will accommodate at grain boundary. The properties of grain boundary were thereby changed, which is considered to be main reason for the decreased t_{ion}. And it is worth to note here that such samples of $Ba_{1.02}Zr_{0.8}Y_{0.2}O_{3-\delta}$ broke into powder after exposure to ambient atmosphere for one week, due to the formation of $BaCO_3$.

4.3 BZY composition for electrolyte application in fuel cells or electrolysis cells

As the electrolyte in fuel cells and electrolysis cells, ionic conductivity above 0.01 Scm^{-1} is necessary [44], from **Fig. 12**, when the Y content is higher than 0.15, such requirement on conductivity can be meeted even at 500 ^oC. Meanwhile, sufficiently high transport number of ionic conduction is another essential criterion. In general, transport number of ionic conduction around 0.9 does not influence

the performance of fuel cells greatly, but it significantly lowers the performance of the electrolysis cells. [45] So, the electrolysis cells ask for the electrolyte material with much higher transport numbers of ionic conduction. If the cells are operated at 500 °C, t_{ion} in wet O_2 is typically higher than 0.9, and even approaching unity, regardless of the Y content. However, if the cells need to be operated at 600 °C, or even higher temperature for small overpotential of electrode reactions, Y content should be around 0.20 to achieve higher t_{ion} and conductivity. In addition, compared with other composition, the BZY samples with the Y content higher than 0.18 shows relatively better sinterability. Although compatibility between thermal and chemical expansion effect is another important aspect, based on the measurements and analysis performed in this work, the best Y content is around 0.20 for BZY with strictly controlled stoichiometric in Ba content.

5. Conclusions

In this work, a thorough investigation on $BaZrO_3$ doped with 10 – 25 mol% Y with an interval of 1 mol% was performed. After sintering at 1600 °C for 24 h, a bimodal microstructure was confirmed for $BaZr_{1-x}Y_xO_{3-\delta}$ (x = 0.10 – 0.15), whereas $BaZr_{1-x}Y_xO_{3-\delta}$ (x = 0.16 – 0.25) shows quite uniform grain size. BZY10, BZY15 and BZY20 were selected and subjected to sintering at different time. Although uniform grain size around 2 and 6 μm were obtained for BZY15 and BZY20, respectively, the bimodal microstructure maintained for BZY10 after sintering at 1600 °C for even 200 h. In addition, the bulk conductivity of BZY10 decreases by nearly one order when the sintering time was

extended from 24 to 40 h. These results indicate that the status of BZY10 is quite sensitive to the history of heat-treatment, calling for special attention when BZY10 is handled. A systematic evaluation on the transport properties was then performed. When the Y content is above 0.15, total conductivity over 0.01 Scm^{-1} is achieved even at 500 ^{o}C. And the transport number of ionic conduction in wet oxygen increases with the Y content increasing from 0.10 to 0.20, but does not further increase when the Y content is higher than 0.20. And notably, both Ba-deficiency and Ba-excess, deviating from the stoichiometric value of unity, result in decrease in the transport numbers of ionic conduction in wet oxygen. Based on all the information collected in this work, Y content around 0.20 seems to be the optimal composition for BZY to be applied as an electrolyte in fuel cells or electrolysis cells.

Acknowledgements

This work was supported by Sumitomo Electric Industries, Ltd. and the New Energy and Industrial Technology Development Organization (NEDO) in Japan (Project code P14004).

References

1 H. Iwahara, T. Esaka, H. Uchida and N. Maeda, *Solid State Ionics*, 1981, **3-4**, 359.

2 H. Iwahara, H. Uchida and S. Tanaka, *Solid State Ionics*, 1983, **9-10**, 1021.

3 C. Kokkofitis, M. Ouzounidou, A. Skodra and M. Stoukides, *Solid State Ionics*, 2007, **178**, 507.

4 L. Bi and E. Traversa, *J. Mater. Res.*, 2014, **29**, 1.

5 N. Kochetova, I. Animista, D. Medvedev, A. Demin and P. Tsiakaras, *RSC Adv.*, 2016, **6**, 73222.

6 S. Hossain, A.M. Abdalla, S.N.B. Jamain, J.H. Zaini and A.K. Azad, *Renew. Sust. Energ. Rev.*, 2017, **79**, 750.

7 Y. Yamazaki, R. Hernandez-Sanchez and S.M. Haile, *Chem. Mater.*, 2009, **21**, 2755.

8 D. Han, N. Hatada and T. Uda, *J. Am. Ceram. Soc.*, 2016, **99**, 3745.

9 K. Katahira, Y. Kohchi, T. Shimura and H. Iwahara, *Solid State Ionics*, 2000, **138**, 91.

10 Y. Guo, Y. Lin, H. Shi, R. Ran and Z. Shao, *Chin, J. Catal.*, 2009, **30**, 479.

11 Y. Okumura, Y. Nose, J. Katayama and T. Uda, *J. Electrochem. Soc.*, 2011, **158**, B1067.

12 L. Bi, E. Fabbri, Z. Sun and E. Traversa, *Energy Environ. Sci.*, 2011, **4**, 1352.

13 C. Duan, J. Tong, M. Shang, S. Nikodemski, M. Sanders, S. Ricote, A. Almansoori and R. O'Hayre, *Science*, 2015, **349**, 1321.

14 K. Bae, D.Y. Jang, H.J. Choi, D. Kim, J. Hong, B. Kim, J. Lee, J. Son and J.H. Shim, *Nat. Commun.*, 2017, 14553.

15 L. Bi, S.P. Shafi and E. Traversa, *J. Mater. Chem. A*, 2015, **3**, 5815.

16 L. Lei, Z. Tao, X. Wang, J.P. Lemmon and F. Chen, *J. Mater. Chem. A*, 2017, **5**, 22945.

17 M. Fountaine, W. Xing, Z. Li, R. Strandbakke, C. Denonville, T. Norby and R. Bredesen, *18th International Conference on Solid State Protonic Conductors*, Oslo, Norway, 2016.

18 Stefan, M. Stange, C. Denonville, Y. Larring, N. Hildenbrand, T. Norby and R. Hausgrud, *J. Mater.*

Sci., 2017, **52**, 6486.

19 L. Bi, E.H. Da'as, S.P. Shafi, *Electrochem. Commun*., 2017, **80**, 20.

20 H. Bae, J. Choi, K. Kim, D. Park, G. Choi, *Int. J. Hydrogen Energy*, 2015, **40**, 2775.

21 H. Bae, G. Choi, *J. Power Sources*, 2015, **285**, 431.

22 Onishi, D. Han, Y. Noda, N. Hatada, M. Majima and T. Uda, *Solid State Ionics*, 2018, **317**, 127.

23 E. Fabbri, D. Pergolesi, S. Licoccia, E. Traversa, *Solid State Ionics*, 2010, **181**, 1043.

24 D. Han, Y. Noda, T. Onishi, N. Hatada, M. Majima and T. Uda, *Int. J. Hydrogen Energy*, 2016, **41**, 14897.

25 K. Nomura, H. Kageyama, *Solid State Ionics*, 2007, **178**, 661.

26 A.V. Kuz'min, V.B. Balakireva, S.V. Plaksin, V.P. Gorelov, *Rus. J. Electrochem*., 2009, **45**, 1351.

27 H. Zhu, S. Ricote, W.G. Coors, R.J. Kee, *Faraday Discuss*., 2015, **182**, 49.

28 K. Kato, D. Han and T. Uda, *J. Am. Ceram. Soc*., 2018, DOI: 10.1111/jace.15946.

29 D. Han, K. Kishida, K. Shinoda, H. Inui and T. Uda, *J. Mater. Chem. A*, 2013, **1**, 3027.

30 D. Han, K. Shinoda, S. Sato, M. Majima and T. Uda, *J. Mater. Chem. A*, 2015, **3**, 1243.

31 S. Imashuku, T. Uda, Y. Nose and Y. Awakura, *J. Phase Equilib. Diff*., 2010, **31**, 348.

32 D. Han, Y. Nose, K. Shinoda and T. Uda, *Solid State Ionics*, 2012, **213**, 2.

33 R.D. Shannon, *Acta Crystallogr. A*, 1976, **32**, 751.

34 S. Imashuku, T. Uda, Y. Nose and Y. Awakura, *J. Alloys Compd*., 2011, **509**, 3872.

35 D. Han, K. Shinoda, S. Tsukimoto, H. Takeuchi, C. Hiraiwa, M. Majima and T. Uda, *J. Mater.*

Chem. A, 2014, **2**, 12552.

36 A.K. Azad, C. Savaniu, S. Tao, S. Duval, P. Holtappels, R.M. Ibberson and J.T.S. Irvine, *J. Mater. Chem.*, 2008, **18**, 3414.

37 P. Babilo, T. Uda and S.M. Haile, *J. Mater. Res.*, 2007, **22**, 1322.

38 D. Han, K. Kishida, H. Inui and T. Uda, *RSC Adv.*, 2014, **4**, 31589.

39 H.G. Bohn and T. Schober, *J. Am. Cera. Soc*., 2000, **83**, 768.

40 C. Kjølseth, H. Fjeld, Ø. Prytz, P.I. Dahl, C. Estournès, R. Haugsrud and T. Norby, *Solid State Ionics*, 2010, **181**, 268.

41 M. Liu and H. Hu, *J. Electrochem. Soc.*, 1996, **143**, L109.

42 V.V. Kharton and F.M.B. Marques, *Solid State Ionics*, 2001, **140**, 381.

43 Y. Yamazaki, R. Hernandez-Sanchez and S.M. Haile, *J. Mater Chem*., 2010, **20**, 8158.

44 B.C.H. Steele and A. Heinzel, *Nature*, 2001, **414**, 345.

45 T. Onishi and T. Uda, in preparation.

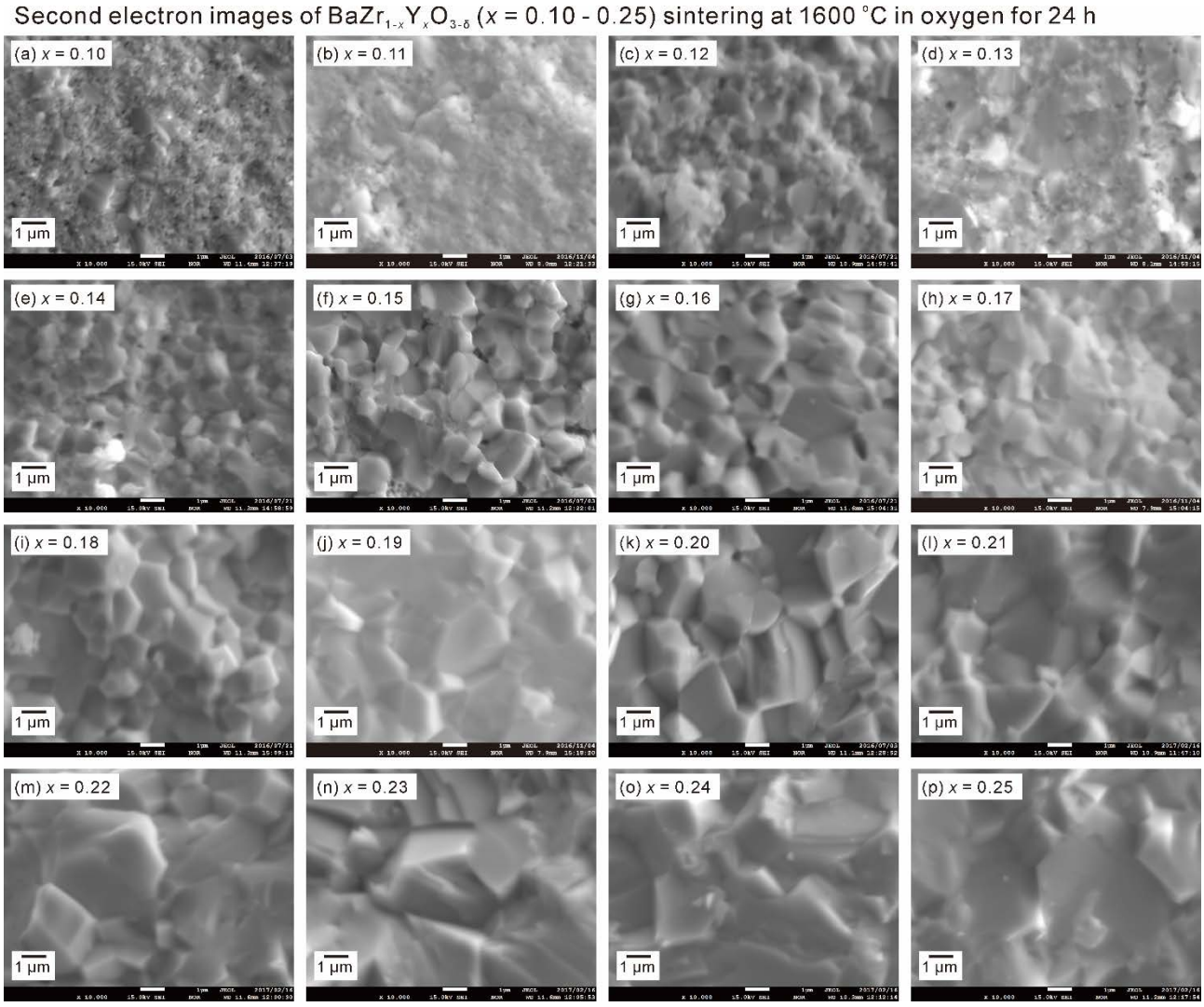

Fig. 1 EPMA second electron images of fractured cross-section area of as-sintered $BaZrO_3$ doped with various amount of Y. All the samples were sintered at 1600 ºC in oxygen for 24 h, and furnace cooled to room temperature, except for $BaZr_{0.8}Y_{0.2}O_{3-\delta}$ which was quenched in the ambient atmosphere.

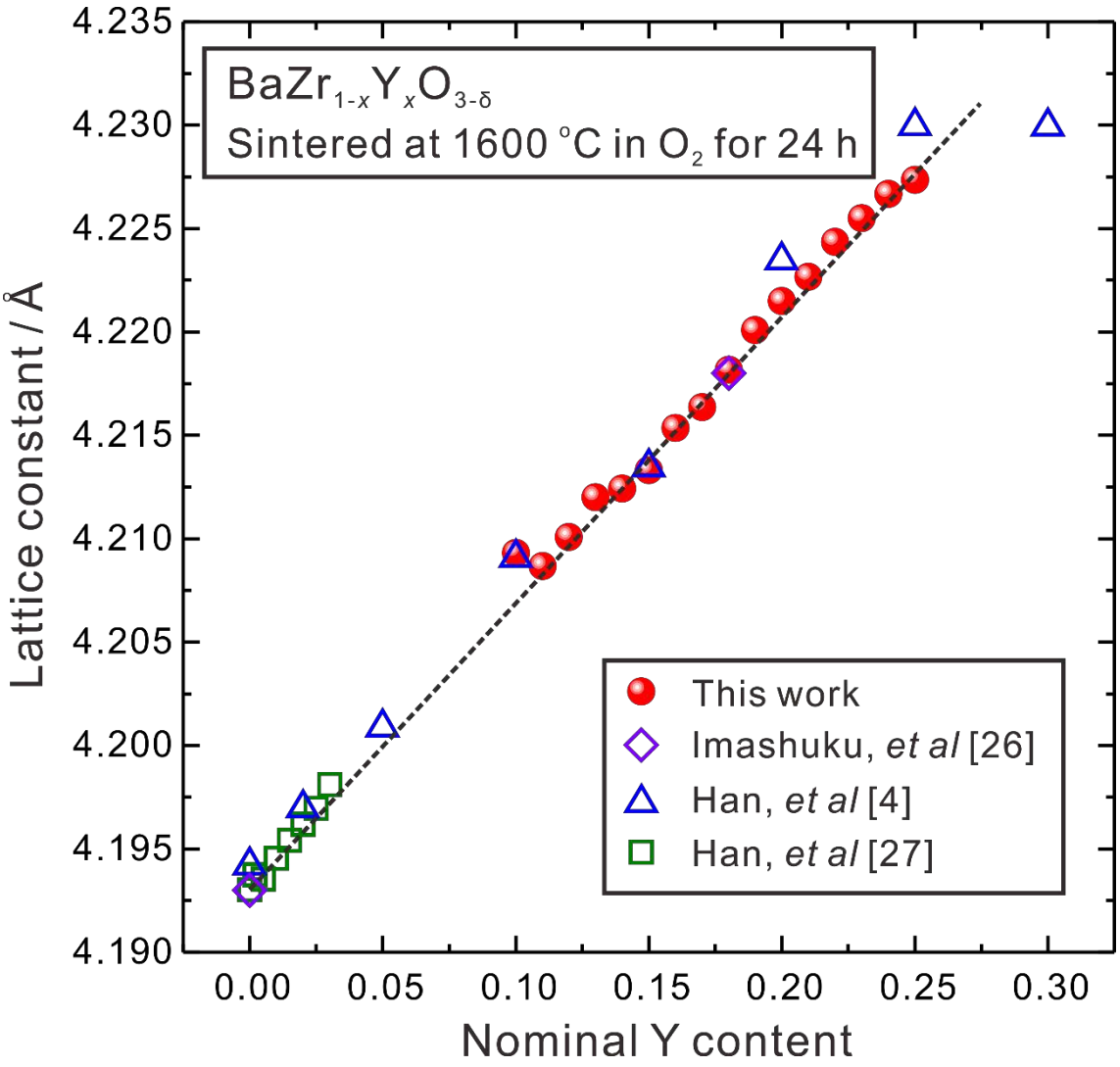

Fig. 2 Lattice constants of the as-sintered $BaZrO_3$ doped with various amount of Y. All the samples were sintered at 1600 ºC in oxygen for 24 h.

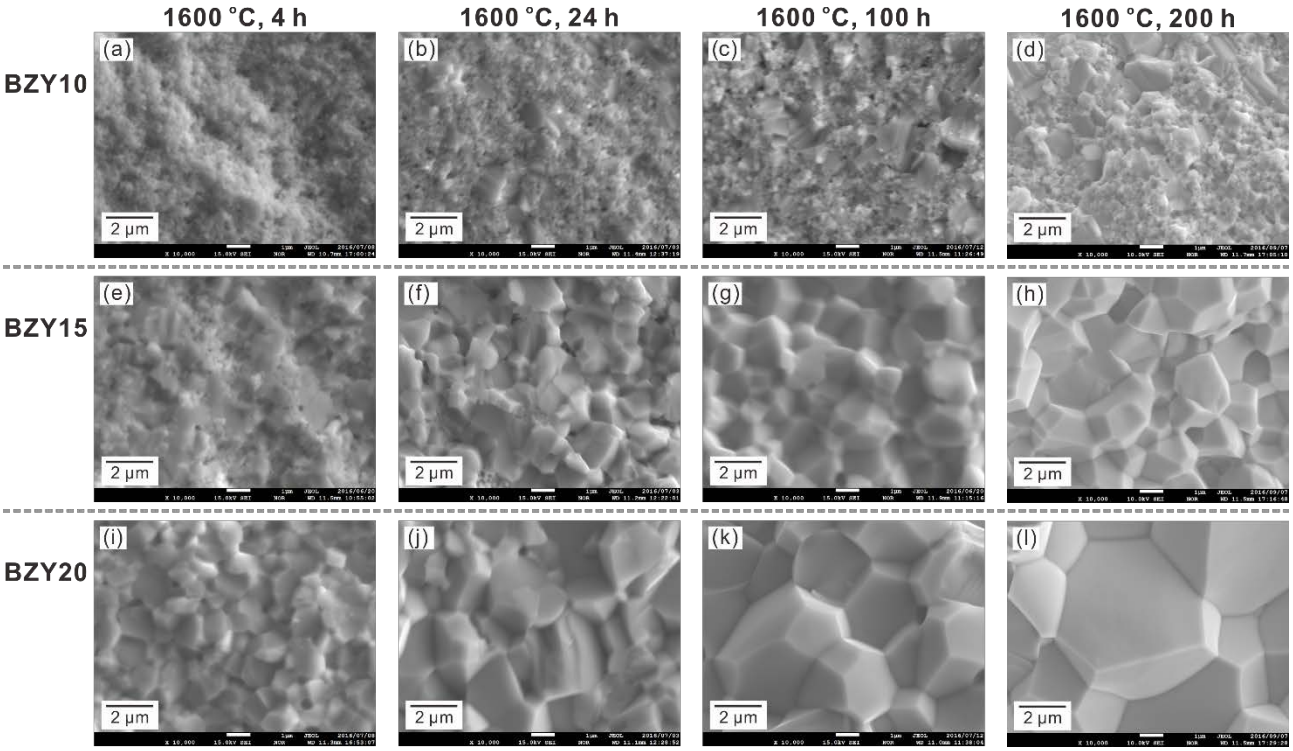

Fig. 3 EPMA second electron images of $BaZr_{0.9}Y_{0.1}O_{3-\delta}$, $BaZr_{0.85}Y_{0.15}O_{3-\delta}$ and $BaZr_{0.8}Y_{0.2}O_{3-\delta}$ sintered at 1600 ^{o}C for 4, 24, 100 or 200 h. All the samples were subsequently quenched in ambient atmosphere.

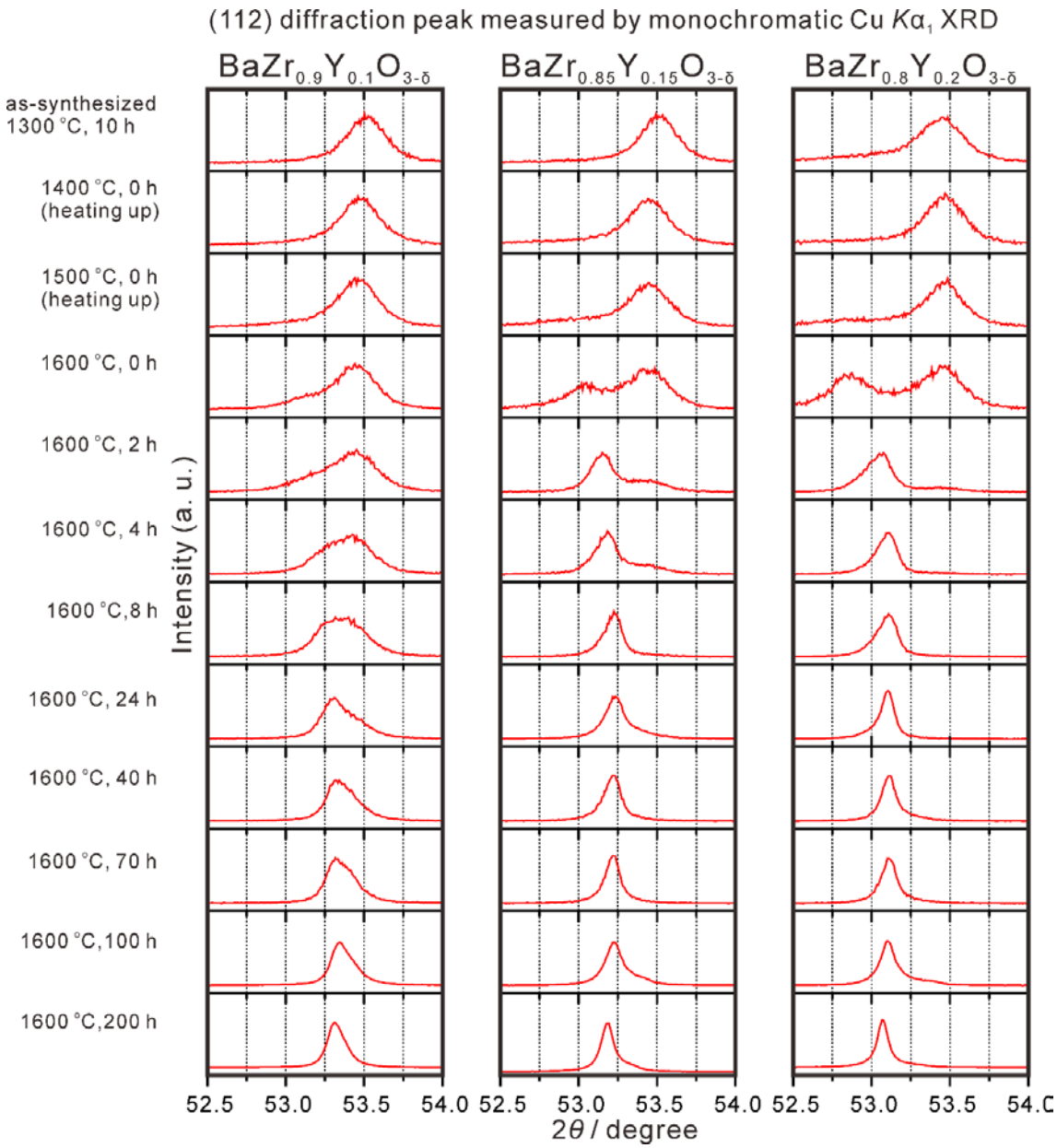

Fig. 4 Change in shape of (112) diffraction peaks collected with monochromatic Cu *K*α1 radiation of $BaZr_{0.9}Y_{0.1}O_{3-\delta}$, $BaZr_{0.85}Y_{0.15}O_{3-\delta}$ and $BaZr_{0.8}Y_{0.2}O_{3-\delta}$ during the heat-treatment for sintering at 1600 °C. The samples were heated up at 4.17 °Cmin^{-1} from room temperature to 1000 °C, and 3.33 °Cmin^{-1} from 1000 to 1600 °C. After holding at 1600 °C for up to 200 h, all the samples were quenched in ambient atmosphere.

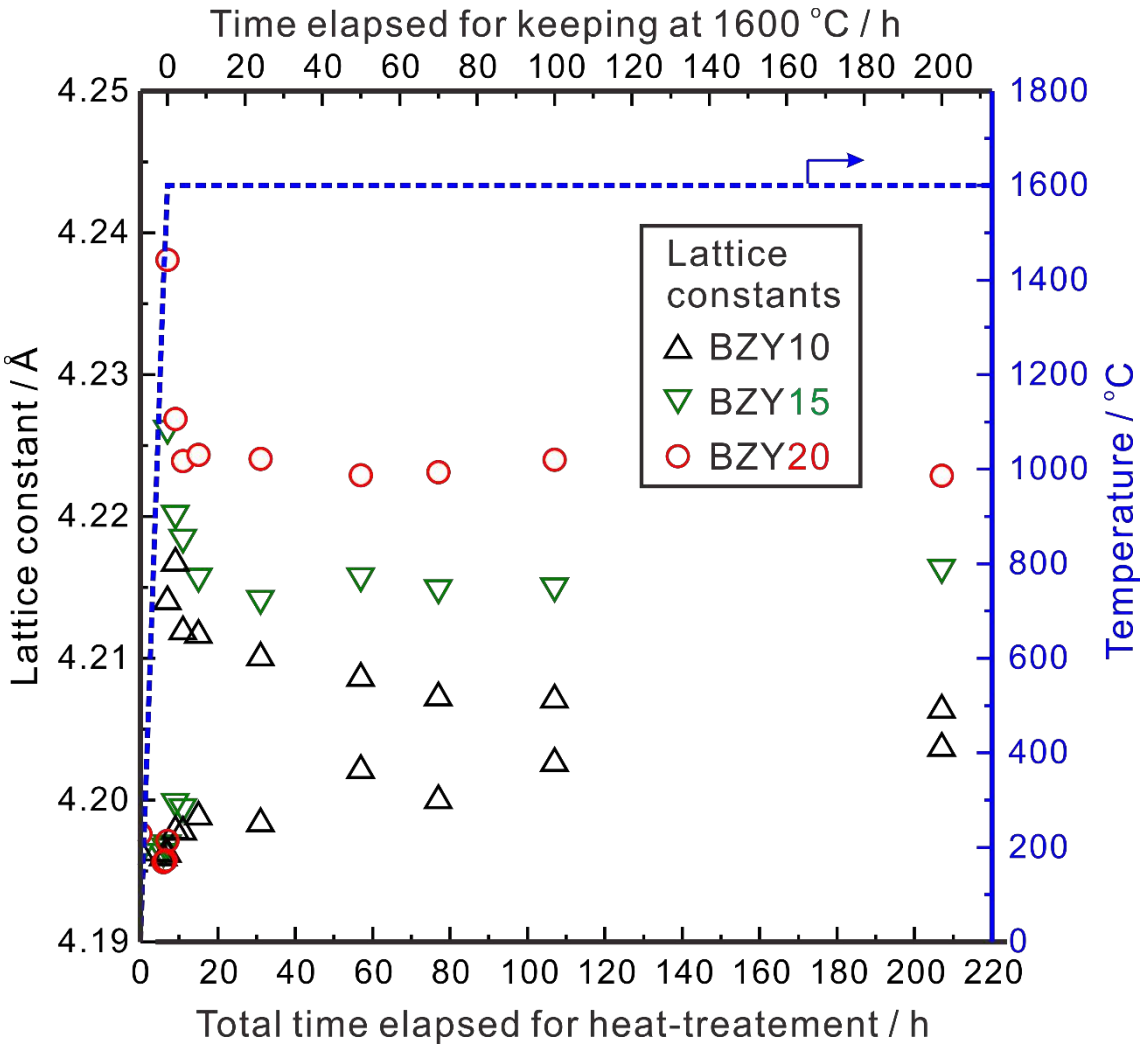

Fig. 5 Change of lattice constants of perovskite phases in $BaZr_{0.9}Y_{0.1}O_{3-\delta}$ (BZY10), $BaZr_{0.85}Y_{0.15}O_{3-\delta}$ (BZY15) and $BaZr_{0.8}Y_{0.2}O_{3-\delta}$ (BZY20) with proceeding of the sintering process. The samples were heated up at 4.17 $^{o}Cmin^{-1}$ from room temperature to 1000 ^{o}C, and 3.33 $^{o}Cmin^{-1}$ from 1000 to 1600 ^{o}C, and held at 1600 ^{o}C for up to 200 h. All the samples were quenched in ambient atmosphere.

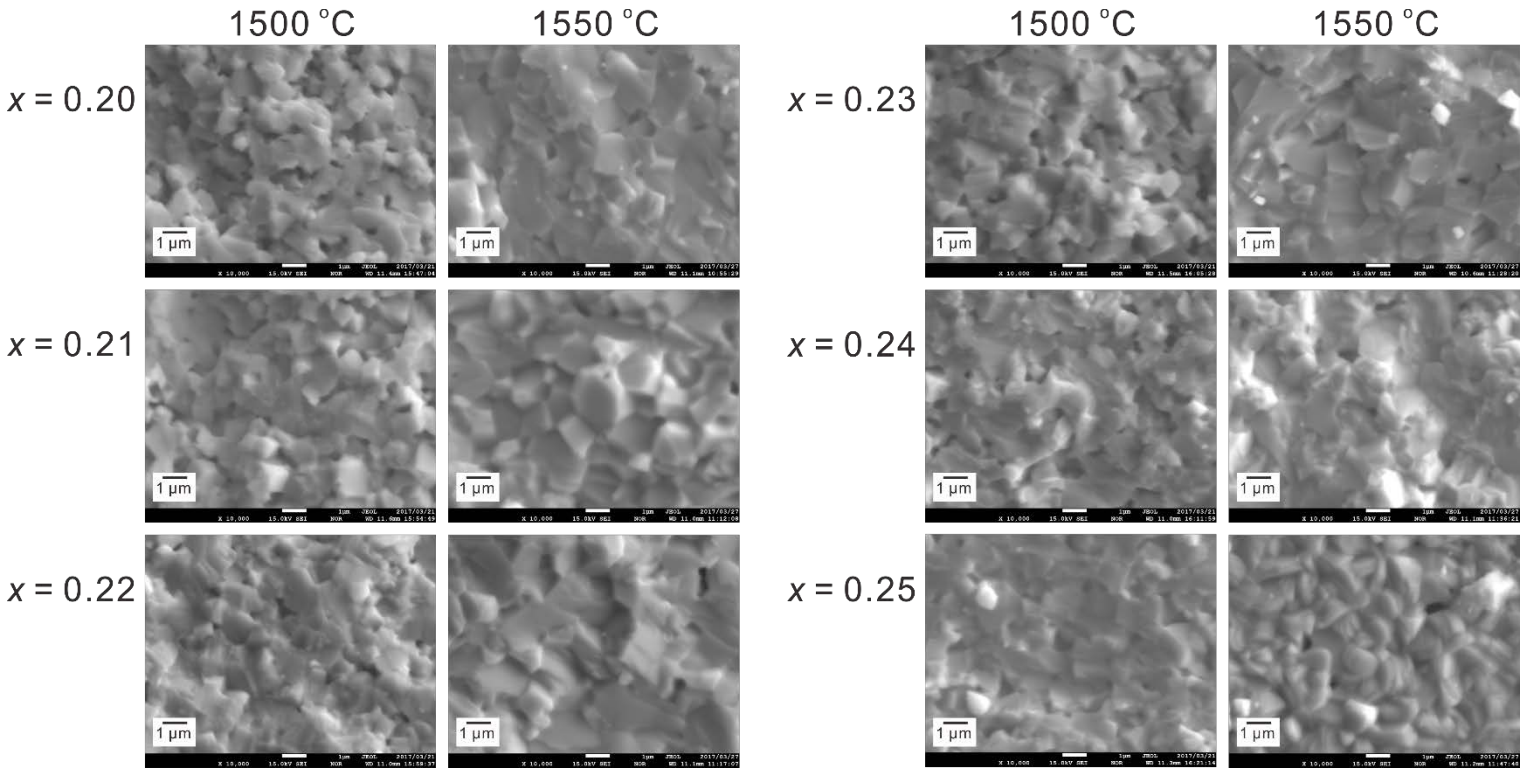

Fig. 6 EPMA second electron images of fracture cross-section area of $BaZr_{1-x}Y_xO_{3-\delta}$ (x = 0.20, 0.21, 0.22, 0.23, 0.24 and 0.25) sintered at 1500 or 1550 °C in oxygen for 24. All the samples were furnace cooled to room temperature.

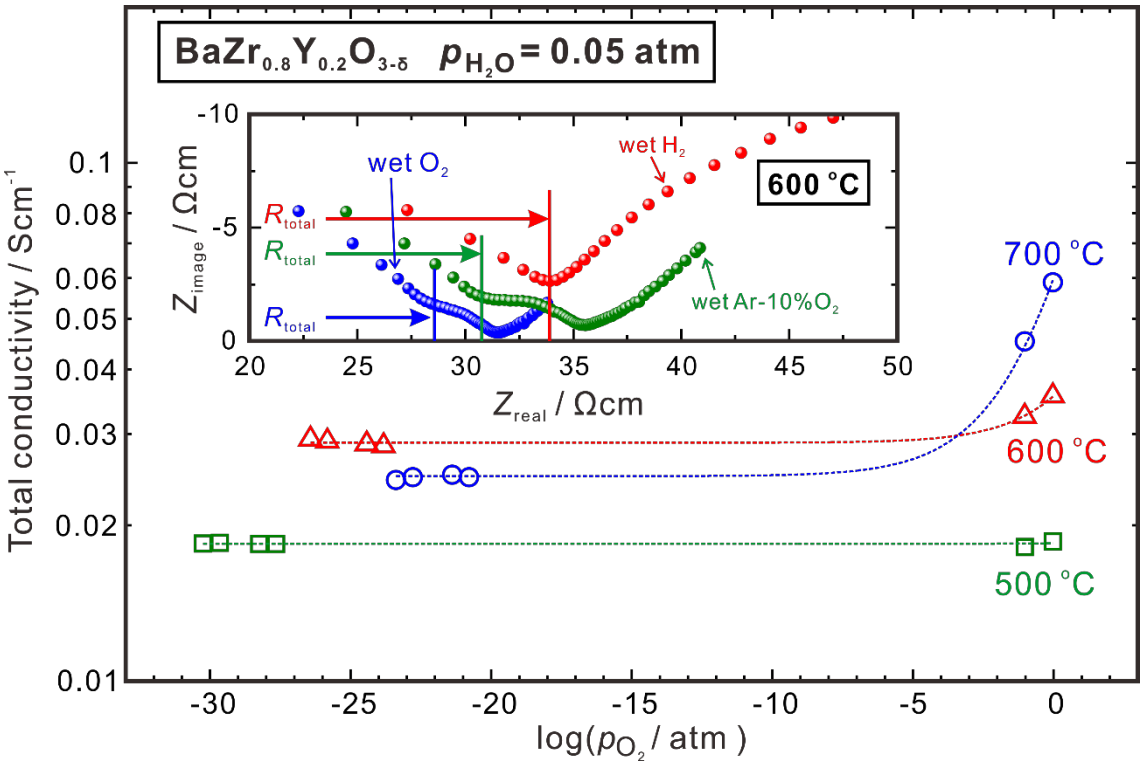

Fig. 7 Dependence of total conductivity of nominally stoichiometric $BaZr_{0.8}Y_{0.2}O_{3-\delta}$ on partial pressure of oxygen at 500, 600 and 700 °C. The impedance spectra at 600 °C in wet H_2, Ar – 10% O_2, and O_2 are given in the inset to show how the total resistance were determined. The sample was sintered at 1600 °C in oxygen for 24 h and quenched to room temperature. The partial pressure of water vapor in the atmosphere for collecting the impedance spectra was 0.05 atm. The composition of the sample was determined to be $Ba_{0.99}Zr_{0.80}Y_{0.20}O_{3-\delta}$ by ICP-AES measurement.

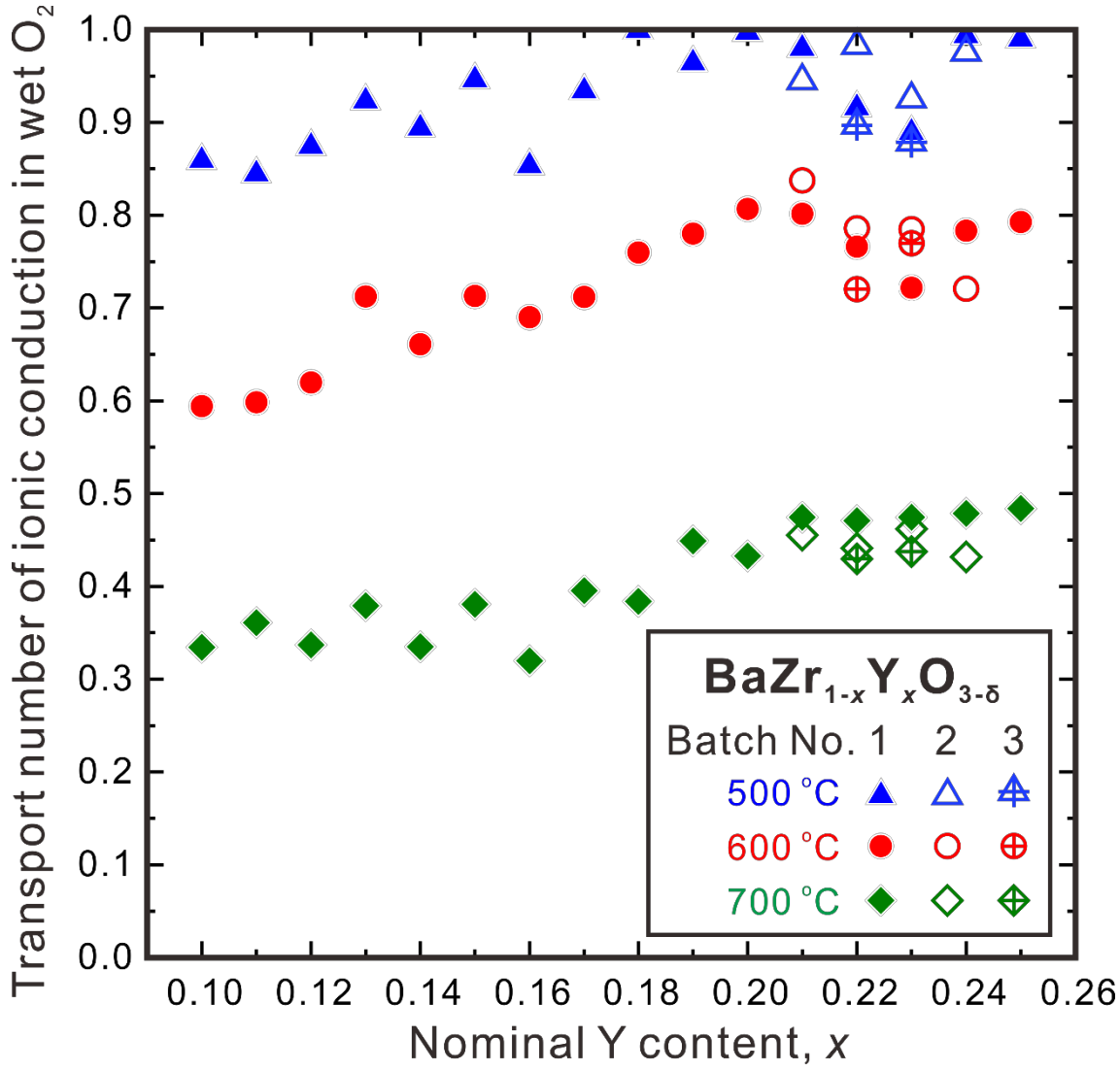

Fig. 8 Transport numbers of ionic conduction in wet O_2 (p_{H_2O} = 0.05 atm) in the nominally stoichiometric $BaZrO_3$ doped with various amount of Y. Additional batches of samples of $BaZr_{1-x}Y_xO_{3-\delta}$ (x = 0.21, 0.22 0.23, 0.24) were prepared and tested to check the reproducibility.

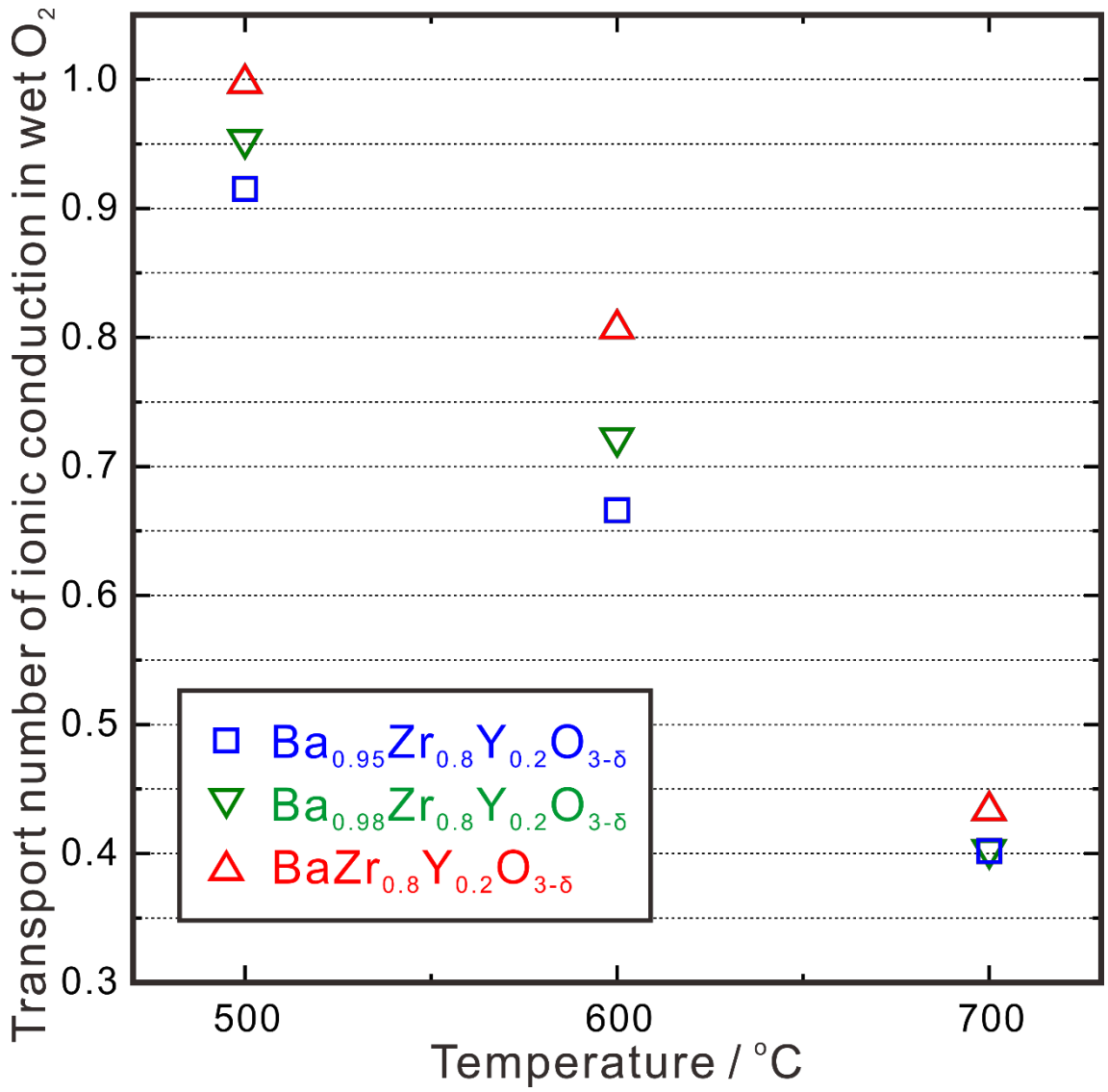

Fig. 9 Transport numbers of ionic conduction in stoichiometric $BaZr_{0.8}Y_{0.2}O_{3-\delta}$, and Ba-deficient samples of $Ba_{0.95}Zr_{0.8}Y_{0.2}O_{3-\delta}$ and $Ba_{0.98}Zr_{0.8}Y_{0.2}O_{3-\delta}$ in wet O_2 (p_{H_2O} = 0.05 atm). All the samples were finally heat-treated at 1600 °C in oxygen for 24 h. The Ba-deficient samples were furnace cooled to room temperature, whereas the stoichiometric sample was quenched in ambient atmosphere.

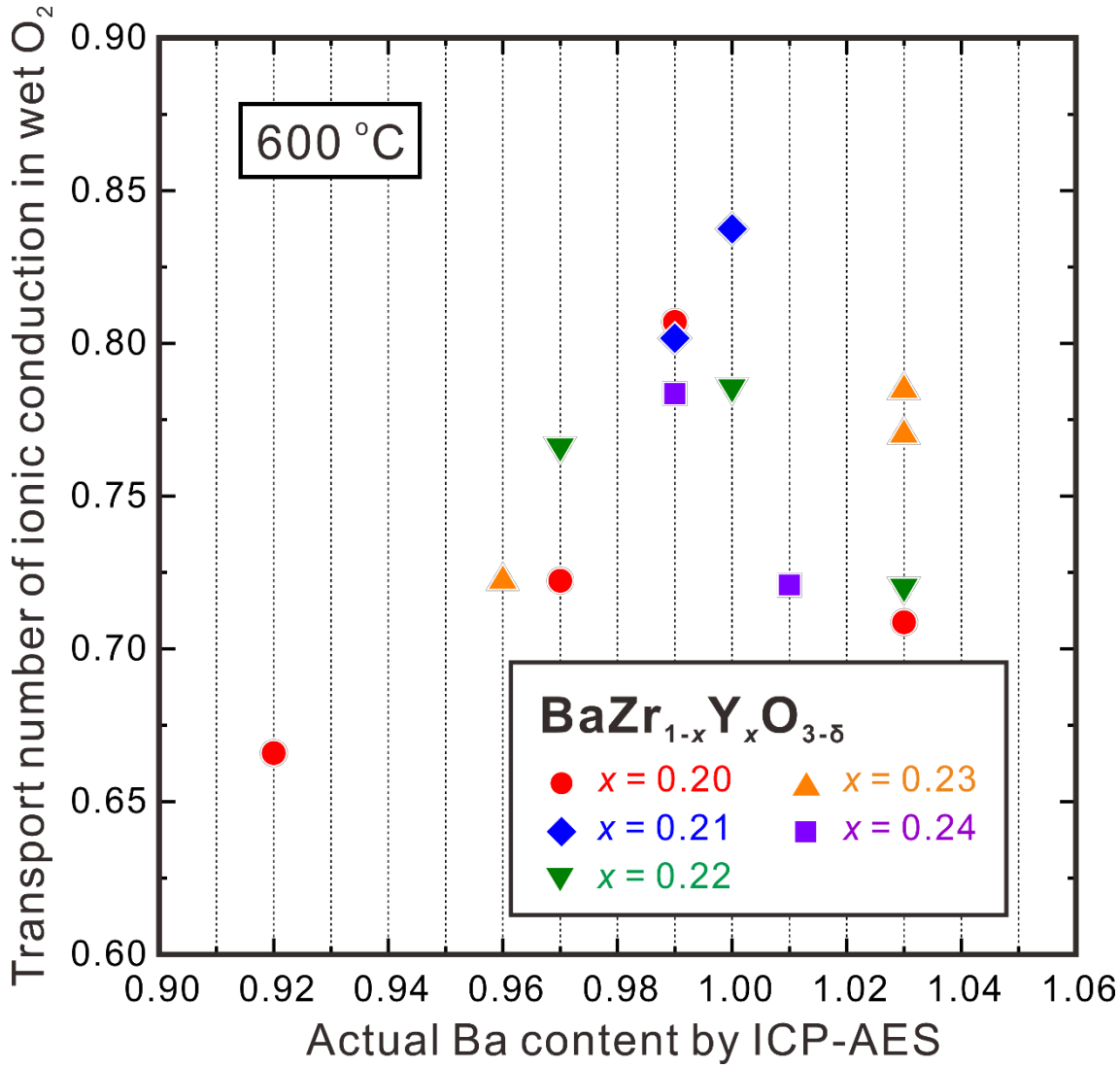

Fig. 10 Transport numbers of ionic conduction at 600 °C in wet O_2 (p_{H_2O} = 0.05 atm) of $BaZr_{1-x}Y_xO_{3-\delta}$ (x = 0.20, 0.21, 0.22 0.23, 0.24) plotted against the actual Ba content determined by ICP-AES measurements.

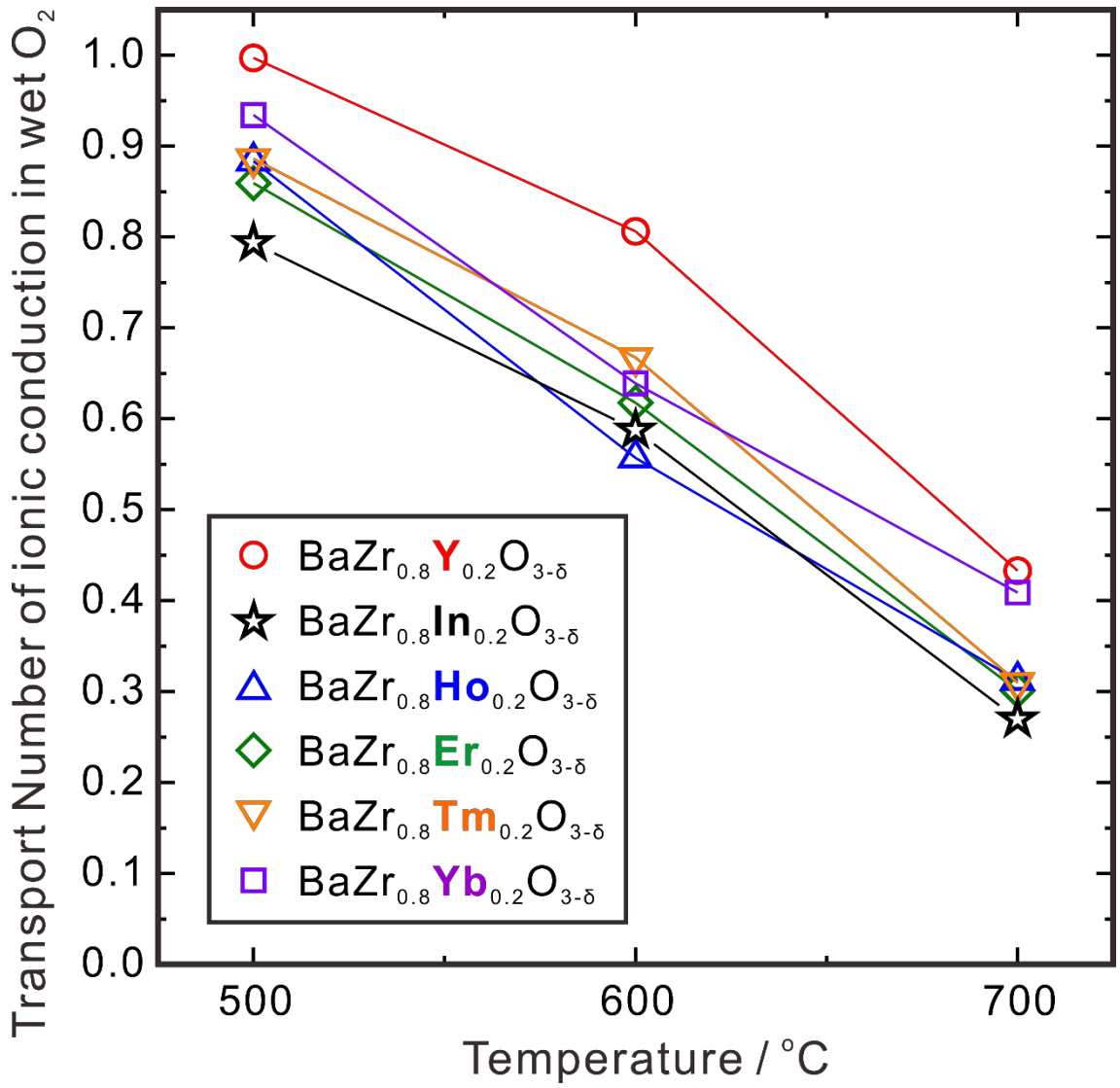

Fig. 11 Transport numbers of ionic conduction in nominally stoichiometric $BaZr_{0.8}M_{0.2}O_{3-\delta}$ (M = Y, In, Ho, Er, Tm and Yb) in wet O_2 (p_{H_2O} = 0.05 atm). All the samples were finally heat-treated at 1600 °C in oxygen for 24 h. All samples were furnace cooled to room temperature, except $BaZr_{0.8}Y_{0.2}O_{3-\delta}$ which was quenched in ambient atmosphere.

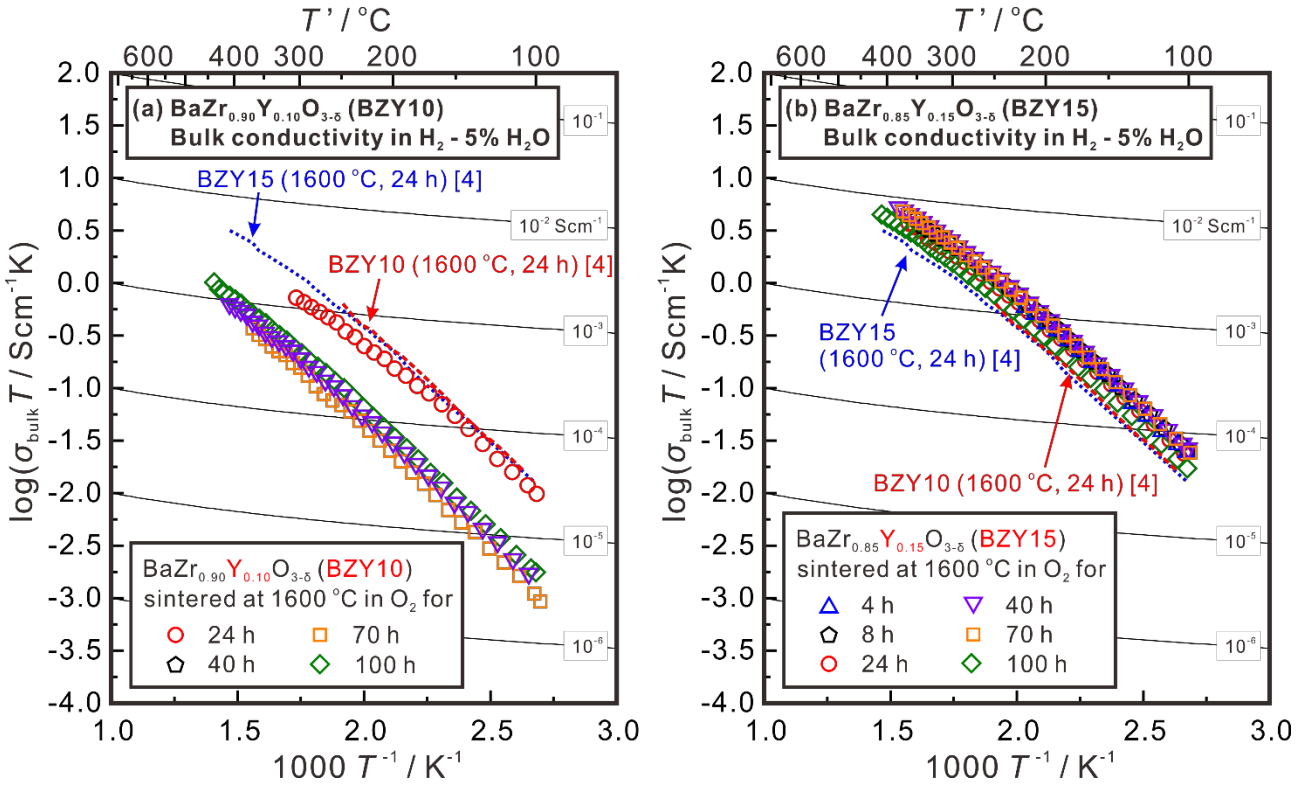

Fig. 12 Arrhenius plots of bulk conductivity in wet H_2 (p_{H_2O} = 0.05 atm) of (a) $BaZr_{0.9}Y_{0.1}O_{3-\delta}$, and (b) $BaZr_{0.85}Y_{0.15}O_{3-\delta}$ heat-treated at 1600 °C for various time for sintering. All the samples were finally quenched in ambient atmosphere.

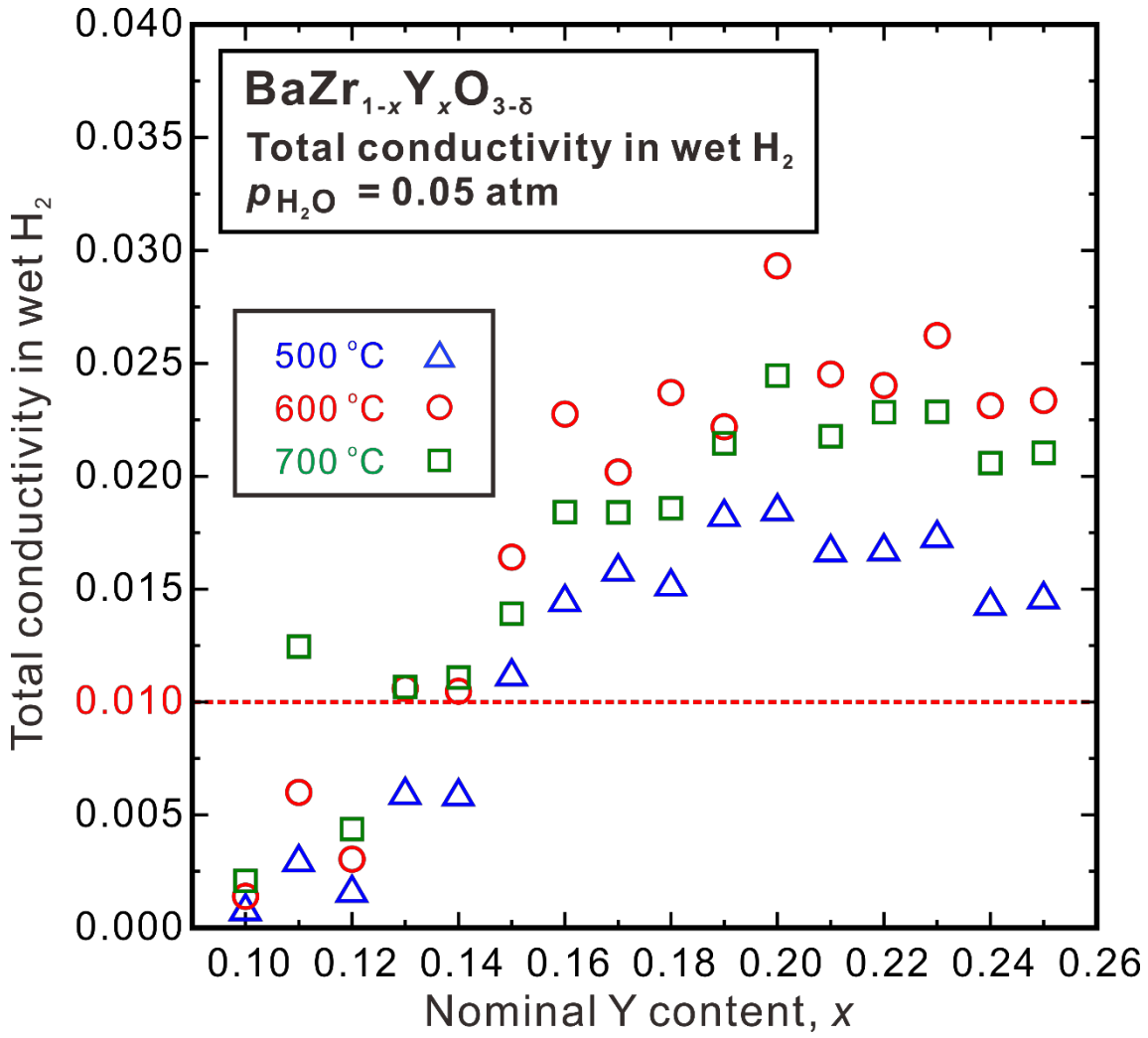

Fig. 13 Total conductivity of $BaZrO_3$ doped with various amount of Y in wet H_2 (p_{H_2O} = 0.05 atm) at 500, 600 and 700 °C. All the samples were sintered at 1600 °C in oxygen for 24 h.

Table 1 Actual composition of stoichiometric $BaZr_{1-x}Y_xO_{3-\delta}$ of three batches, Ba-deficient or excessive $BaZr_{0.8}Y_{0.2}O_{3-\delta}$, and $BaZr_{0.8}M_{0.2}O_{3-\delta}$ (M = In, Ho, Er, Tm, Yb) determined by ICP-AES measurements.

Batch No.	Nominal Composition	Actual Composition	Batch No.	Nominal Composition	Actual Composition
1	$BaZr_{0.90}Y_{0.10}O_{3-\delta}$	$Ba_{1.00}Zr_{0.90}Y_{0.10}O_{3-\delta}$	1	$BaZr_{0.82}Y_{0.18}O_{3-\delta}$	$Ba_{0.98}Zr_{0.82}Y_{0.18}O_{3-\delta}$
	$BaZr_{0.89}Y_{0.11}O_{3-\delta}$	$Ba_{1.03}Zr_{0.89}Y_{0.11}O_{3-\delta}$		$BaZr_{0.81}Y_{0.19}O_{3-\delta}$	$Ba_{1.01}Zr_{0.81}Y_{0.19}O_{3-\delta}$
	$BaZr_{0.88}Y_{0.12}O_{3-\delta}$	$Ba_{1.03}Zr_{0.88}Y_{0.12}O_{3-\delta}$		$BaZr_{0.80}Y_{0.20}O_{3-\delta}$	$Ba_{0.99}Zr_{0.80}Y_{0.20}O_{3-\delta}$
	$BaZr_{0.87}Y_{0.13}O_{3-\delta}$	$Ba_{1.05}Zr_{0.87}Y_{0.13}O_{3-\delta}$		$BaZr_{0.79}Y_{0.21}O_{3-\delta}$	$Ba_{0.99}Zr_{0.79}Y_{0.21}O_{3-\delta}$
	$BaZr_{0.86}Y_{0.14}O_{3-\delta}$	$Ba_{1.06}Zr_{0.86}Y_{0.14}O_{3-\delta}$		$BaZr_{0.78}Y_{0.22}O_{3-\delta}$	$Ba_{0.97}Zr_{0.78}Y_{0.22}O_{3-\delta}$
	$BaZr_{0.85}Y_{0.15}O_{3-\delta}$	$Ba_{1.03}Zr_{0.85}Y_{0.15}O_{3-\delta}$		$BaZr_{0.77}Y_{0.23}O_{3-\delta}$	$Ba_{0.96}Zr_{0.77}Y_{0.23}O_{3-\delta}$
	$BaZr_{0.84}Y_{0.16}O_{3-\delta}$	$Ba_{1.00}Zr_{0.84}Y_{0.16}O_{3-\delta}$		$BaZr_{0.76}Y_{0.24}O_{3-\delta}$	$Ba_{0.99}Zr_{0.76}Y_{0.24}O_{3-\delta}$
	$BaZr_{0.83}Y_{0.17}O_{3-\delta}$	$Ba_{1.05}Zr_{0.83}Y_{0.17}O_{3-\delta}$		$BaZr_{0.75}Y_{0.25}O_{3-\delta}$	$Ba_{0.99}Zr_{0.75}Y_{0.25}O_{3-\delta}$
2	$BaZr_{0.79}Y_{0.21}O_{3-\delta}$	$Ba_{1.00}Zr_{0.79}Y_{0.21}O_{3-\delta}$	2	$BaZr_{0.77}Y_{0.23}O_{3-\delta}$	$Ba_{1.03}Zr_{0.77}Y_{0.23}O_{3-\delta}$
	$BaZr_{0.78}Y_{0.22}O_{3-\delta}$	$Ba_{1.00}Zr_{0.78}Y_{0.22}O_{3-\delta}$		$BaZr_{0.76}Y_{0.24}O_{3-\delta}$	$Ba_{1.01}Zr_{0.76}Y_{0.24}O_{3-\delta}$
3	$BaZr_{0.78}Y_{0.22}O_{3-\delta}$	$Ba_{1.03}Zr_{0.78}Y_{0.22}O_{3-\delta}$	3	$BaZr_{0.77}Y_{0.23}O_{3-\delta}$	$Ba_{1.03}Zr_{0.77}Y_{0.23}O_{3-\delta}$
4	$Ba_{0.95}Zr_{0.80}Y_{0.20}O_{3-\delta}$	$Ba_{0.92}Zr_{0.79}Y_{0.21}O_{3-\delta}$	4	$Ba_{1.02}Zr_{0.80}Y_{0.20}O_{3-\delta}$	$Ba_{1.03}Zr_{0.80}Y_{0.20}O_{3-\delta}$
	$Ba_{0.98}Zr_{0.80}Y_{0.20}O_{3-\delta}$	$Ba_{0.97}Zr_{0.80}Y_{0.20}O_{3-\delta}$			
5	$BaZr_{0.80}In_{0.20}O_{3-\delta}$	$Ba_{1.03}Zr_{0.81}In_{0.19}O_{3-\delta}$	5	$Ba_{1.02}Zr_{0.79}Tm_{0.21}O_{3-\delta}$	$Ba_{1.02}Zr_{0.79}Tm_{0.21}O_{3-\delta}$
	$BaZr_{0.80}Ho_{0.20}O_{3-\delta}$	$Ba_{1.00}Zr_{0.80}Ho_{0.20}O_{3-\delta}$		$Ba_{1.04}Zr_{0.78}Yb_{0.22}O_{3-\delta}$	$Ba_{1.04}Zr_{0.78}Yb_{0.22}O_{3-\delta}$
	$BaZr_{0.80}Er_{0.20}O_{3-\delta}$	$Ba_{0.99}Zr_{0.80}Er_{0.20}O_{3-\delta}$			